

1 **Global Estimation of the Eddy Kinetic Energy**
2 **Dissipation from a Diagnostic Energy Balance**

3 **Romain Torres¹, Robin Waldman¹, Julian Mak^{2,3}, Roland S  f  rian¹**

4 ¹CNRM, Universit   de Toulouse, M  t  o-France, CNRS, Toulouse, France

5 ²Department of Ocean Science, Hong Kong University of Science and Technology, Hong Kong

6 ³Center for Ocean Research in Hong Kong and Macau, Hong Kong University of Science and Technology,
7 Hong Kong

8 **Key Points:**

- 9 • Global mesoscale eddy kinetic energy dissipation rate estimated to 0.66 ± 0.19 TW
10 from observation-based and statistically analysed datasets
- 11 • High dissipation of geostrophic eddies are found in the western boundary currents
12 and the Antarctic Circumpolar Current
- 13 • Estimation of the eddy dissipation timescale from observations to inform future pa-
14 rameterization development

Corresponding author: Romain Torres, romain.torres@meteo.fr

Abstract

Mesoscale eddies regulate the ocean heat and carbon budgets. However, how and where the kinetic energy flows out from the mesoscale reservoir remains uncertain. In this study, a simplified equation of the mesoscale energy budget is used to obtain a global estimation of the eddy dissipation rate. The framework is first validated in a global ocean model and then applied to a density climatology and a global reconstruction of the eddy kinetic energy field. We find a global dissipation rate of 0.66 ± 0.19 TW for the mesoscale kinetic energy, in agreement with recent independent estimates. The results also show an intense dissipation near western boundary currents and in the Antarctic Circumpolar Current, where both large levels of energy and baroclinic conversion occur. The resulting geographical distribution of the dissipation rate brings new insights for closing the ocean kinetic energy budget, as well as constraining future mesoscale parameterizations and associated mixing processes.

Plain Language Summary

The ocean is home to abundant and large swirls from tens to hundreds of kilometers, called “mesoscale eddies”. These eddies contain more momentum than most ocean currents and can thus impact the climate evolution. There are now good reasons to believe the effect of mesoscale eddies are directly related to their strength, and so to their kinetic energy. However, how the energy is removed from these eddies is still unclear mostly due to instrumental and theoretical limitations. In this work, a simplification of the eddy energetic behavior is used to indirectly estimate the dissipation from observations of temperature, salinity and surface currents. Our results confirm intensified dissipation near strong ocean currents and hence constitute a new attempt for the global reconstruction of the eddy kinetic energy dissipation in the world ocean. The work presented here is consistent and complementary to other studies and can help us to understand the ocean energy cycle.

1 Introduction

Oceans play a key role in setting transient climate change (Fox-Kemper et al., 2021), having absorbed the bulk of the excess energy due to anthropogenic emissions (von Schuckmann et al., 2020), redistributing heat across the Earth (Zanna et al., 2019) and affecting sea level rise (Couldrey et al., 2020). The oceans are also a leading component for the anthropogenic carbon uptake (Friedlingstein et al., 2022) and host a diversity of ecosystems and marine resources (Cooley et al., 2022).

Among the many dynamical processes present in the oceans, geostrophic or mesoscale eddies are central in the transport of tracers and can impact on large scale motions. Varying in size from kilometers to hundreds of kilometers, they dominate the oceanic kinetic energy reservoir (Ferrari & Wunsch, 2009) and significantly influence the transport and mixing of water masses in the ocean. While knowledge of the eddy energy field is essential for assessing these properties (Cessi, 2008; Fox-Kemper et al., 2019; Groeskamp et al., 2020), the mesoscale energetics are still not well understood. More precisely, the way the eddy energy dissipates and is transferred toward other scales is complex and poorly constrained by theories and observations. The dissipation of eddy kinetic energy is also associated to the ocean diapycnal mixing through different processes (Naveira Garabato et al., 2004; Saenko et al., 2012; Melet et al., 2015; Yang et al., 2019) and can in turn impact the global overturning circulation (Saenko et al., 2018).

A variety of processes are able to dissipate or transfer the mesoscale mechanical energy. Among them, interactions of geostrophic flow with bottom topography either by direct dissipation drag (Sen et al., 2008; Arbic et al., 2009) and non-propagating form drag (Klymak, 2018; Klymak et al., 2021) or by scattering into lee waves (Nikurashin & Ferrari, 2011) appear to be an important sink of eddy energy. Other candidates include the forward cascade

63 due to instabilities of unbalanced motions (Molemaker et al., 2010; Barkan et al., 2015),
 64 direct interactions with the internal wave field (Polzin, 2010) and suppression by wind work
 65 (Renault et al., 2019; Rai et al., 2021). The reader can refer to the review of McWilliams
 66 (2016) for a more comprehensive description of involved processes.

67 Observational estimates of energy dissipation in the ocean are extremely limited. If some
 68 global quantification exists, large uncertainties remain. The work of Sen et al. (2008) esti-
 69 mates from different observations a global dissipation rate by quadratic bottom boundary
 70 layer drag in the range of 0.2-0.8 TW. The large spread in the estimation is due to hy-
 71 potheses in the calculation of the bottom geostrophic velocities. Regarding other processes,
 72 the lee waves generation rate from geostrophic motion is estimated between 0.2 TW and
 73 0.49 TW (Nikurashin & Ferrari, 2011; Scott et al., 2011) while in a recent study, Rai et
 74 al. (2021) compute a global “eddy killing” rate from the wind of 0.05 TW at scales smaller
 75 than 260 km. Recently, sufficient amount of satellite altimeter data and efficient tracking
 76 algorithms have allowed oceanographers to characterize more systematically eddy properties
 77 (e.g. diameters, direction and lifetimes) both globally (Chelton et al., 2011) and regionally
 78 (Braby et al., 2016; Ji et al., 2018). However, only a few studies derive an overall map of
 79 eddy sinks from these Lagrangian analyses (Zhai et al., 2010; Xu et al., 2011; Sun et al.,
 80 2017).

81 The aim of this paper is to estimate a global dissipation rate of the mesoscale kinetic energy
 82 from observation-based climatology datasets. To do so, a simple diagnostic energy balance
 83 is used, leading to a relation where the eddy dissipation is directly related to the mean ocean
 84 stratification and proportional to the eddy kinetic energy. This relation is first introduced in
 85 section 2. Section 3 proposes a global reconstruction of the mesoscale eddy dissipation rate
 86 using satellite observations and available climatology of temperature and salinity. We finally
 87 discuss the hypotheses of this work in section 4, while section 5 summarizes the implications
 88 and the main conclusions.

89 2 A Simplified Mesoscale Energy Budget

90 We first derive a simplified mesoscale energy balance to retrieve an estimate of the eddy
 91 dissipation. Here we term “dissipation” the energy flux going out to the mesoscale reservoir
 92 although the energy is transferred to other scales, which in turn can provide a route to
 93 dissipation. We use the depth-integral energy budget introduced by the GEOMETRIC
 94 parameterization (Mak et al., 2018) applied to the eddy kinetic energy (EKE):

$$\frac{\partial}{\partial t} \int \text{EKE} \, dz + \underbrace{\nabla_H \cdot \left(\tilde{\mathbf{u}}^z \int \text{EKE} \, dz \right)}_{\text{advection}} = \underbrace{\int \kappa_{gm} \frac{M^4}{N^2} \, dz}_{\text{production}} - \underbrace{\lambda \int \text{EKE} \, dz}_{\text{dissipation}} + \underbrace{\eta_E \nabla_H^2 \int \text{EKE} \, dz}_{\text{diffusion}}, \quad (1)$$

95 where the vertical integration is applied from the bottom to the surface. The depth-
 96 integrated eddy kinetic energy is here advected by the depth-averaged velocity $\tilde{\mathbf{u}}^z$. The
 97 production term is assumed to be dominated by the baroclinic instability (Robinson &
 98 McWilliams, 1974) and represents the eddy growth resulting from isopycnal flattening.
 99 Consistent with the so-called Gent and McWilliams parameterization (Gent & McWilliams,
 100 1990; Gent et al., 1995), it involves an eddy diffusivity coefficient κ_{gm} related to the horizon-
 101 tal and vertical buoyancy stratification, respectively M^2 and N^2 , defined later in Equation
 102 4. For simplicity, all the dissipative processes are approximated as a linear damping at a
 103 rate λ . Finally the eddy energy field is diffused horizontally with the last right hand side
 104 term modulated by a diffusivity η_E . In its original form, GEOMETRIC is a budget for the
 105 total (potential plus kinetic) eddy energy, but in the present study only the kinetic energy
 106 is considered since the baroclinic instability is the main source for the EKE reservoir (von
 107 Storch et al., 2012).

108 Marshall et al. (2012) have proposed a scaling for κ_{gm} where the coefficient is proportional
 109 to the total eddy energy. Again we adapt this framework by using the eddy kinetic energy
 110 only, consistent with the results from Bachman et al. (2017) who find modest differences
 111 when changing the type of energy in the scaling of κ_{gm} . Following the work of Mak et al.
 112 (2018), a two-dimensional formulation is used:

$$\kappa_{gm} = \alpha \frac{\int \text{EKE} dz}{\int (M^2/N) dz}, \quad (2)$$

113 where α is a non-dimensional constant which represents the eddy efficiency to convert mean
 114 available potential energy into mesoscale kinetic energy.

115 We finally simplify the energy budget by assuming a diagnostic balance on decadal time
 116 scales between the baroclinic production and the linear dissipation terms (Marshall et al.,
 117 2017). Then, injecting the scaling of Equation 2 into the production term, both the source
 118 and dissipation terms are now proportional to the depth-integrated EKE. This leads to a
 119 diagnostic relation between the linear eddy dissipation coefficient λ and the ocean stratifi-
 120 cation:

$$\lambda = \alpha \frac{\int (M^4/N^2) dz}{\int (M^2/N) dz}. \quad (3)$$

121 Within this simple energy balance, the eddy dissipation coefficient is a function of the ocean
 122 large scale stratification and the eddy efficiency α only. In this study, we focus on the
 123 simple case where α has no time and spatial dependence and we choose $\alpha = 0.1$ deduced
 124 from previous studies (Marshall et al., 2012; Bachman et al., 2017; Mak et al., 2018; Poulsen
 125 et al., 2019; Wei et al., 2022; Mak, Marshall, et al., 2022). See section 4 for a discussion on
 126 the value of α .

127 In the work of Marshall et al. (2017) and Mak et al. (2017), a similar energy balance
 128 is considered (their Equations 6 and 20 respectively) but used for a different purpose in
 129 order to diagnose the emergent eddy saturation in idealized configurations. They employed
 130 circumpolar domains where the advection and the diffusion of EKE naturally vanish. In
 131 the following, a more local approach is used and the eddy energy balance in Equation 3 is
 132 considered regionally, at a typical scale of $\mathcal{O}(1000)$ km.

133 The eddy energy balance is first validated within a global ocean model (see Text S1 of
 134 the Supporting Information for details of the numerical configuration). To summarize, the
 135 stand-alone ocean simulation includes the GEOMETRIC parameterization (Mak, Marshall,
 136 et al., 2022) which discretizes the Equation 1. Monthly means of model outputs, including
 137 each EKE trends, are stored and used to evaluate the validity of the eddy energy balance. In
 138 accordance with the climatology used in section 3, the simulation outputs are analysed over
 139 the 23-year period from 1995 to 2017. We find a slight dominance of the dissipation term
 140 over the production, leading to a modest underestimation of the eddy dissipation coefficient
 141 λ . However, the proposed diagnostic eddy energy balance is overall valid when analysing
 142 the remaining terms of Equation 1 (see Figures S1 and S2 of the Supporting Information),
 143 allowing the use of a time-averaged stratification to compute the coefficient λ . Finally, we
 144 estimate a mean relative error of 35% on the coefficient λ , a figure used to compute the
 145 uncertainty range in our results (see error and uncertainty quantification in Text S1 of the
 146 Supporting Information).

147 3 Eddy Dissipation from global Observations

148 3.1 Datasets

149 Retrieving the eddy dissipation rate from Equation 3 only requires an averaged large-scale
 150 density field from which the ocean stratification can be computed. For that, we use the
 151 in-situ temperature and practical salinity reconstructions from the World Ocean Atlas 2018
 152 (WOA18) climatology (Garcia et al., 2019) to compute the conservative temperature Θ , the
 153 absolute salinity S_A and the in-situ density ρ using the TEOS-10 equation of state (IOC et
 154 al., 2010) from the GSW python toolbox (Firing et al., 2021). Then, both horizontal and
 155 vertical stratifications M^2 and N^2 are computed as:

$$M^2 = \frac{g}{\rho_0} |\nabla_h \rho|, \quad N^2 = \frac{g}{\rho_0} \left(\alpha_\Theta \frac{\partial \Theta}{\partial z} - \beta_s \frac{\partial S_A}{\partial z} \right), \quad (4)$$

156 with g the gravity acceleration, $\rho_0 = 1026 \text{ kg/m}^3$ a reference density, and α_Θ and β_s the
 157 seawater thermal expansion and saline contraction coefficients respectively. A relatively
 158 large time span climatological mean is needed as the balance Equation 3 is valid typically
 159 at the large-scale and over decadal timescales. We therefore use a merge of two WOA18
 160 datasets covering a 23-year period from 1995 to 2017, which incorporates the global Argo
 161 float measurements from 2005.

162 An estimation of the EKE is required to deduce the final dissipation rate defined by the sec-
 163 ond right hand side term in Equation 1. Similar to the work of Groeskamp et al. (2020), we
 164 compute the surface eddy kinetic energy from sea surface geostrophic velocity anomalies (u'_0 ,
 165 v'_0) with respect to the 1995-2017 period and collected at $1/4^\circ$ resolution from the European
 166 Union-Copernicus Marine Service (2021). The resulting EKE map is then regridded onto
 167 the WOA18 grid while ensuring energy conservation. Since a three-dimensional energy field
 168 is needed, we apply a vertical structure function assumed to be separable so that the eddy
 169 velocity components can be formulated as $(u', v') = \phi(z)(u'_0, v'_0)$. The structure function
 170 $\phi(z)$ assumes a rough bottom topography (LaCasce & Groeskamp, 2020) and is found by
 171 solving a differential equation throughout the water column (see calculation details in Text
 172 S2 of the Supporting Information). The function $\phi(z)$ represents the variation of the eddy
 173 velocity with depth and is used to compute the depth-integrated EKE:

$$\int \text{EKE} dz = \int \frac{(u_0'^2 + v_0'^2)}{2} \phi(z)^2 dz. \quad (5)$$

174 3.2 The Eddy Dissipation Timescale

175 From the WOA18 dataset, both the horizontal and vertical stratifications are computed.
 176 The integral of these metrics over the whole depth is mapped in Figure 1a,b. The horizontal
 177 stratification turns out to be a good proxy for the shear found in strong oceanic baro-
 178 clinic currents, notably western boundary currents and the Antarctic Circumpolar Current
 179 (ACC). To a lesser extent, it also shows the subtropical gyre signatures and their western
 180 intensification. We also note extreme and noisy values at high latitudes, especially in the
 181 Arctic Ocean, likely due to a lack of observations during winter in the WOA18 dataset.
 182 On the other hand, the vertical stratification map shows a general equatorward increase,
 183 with regionally reduced stratification over eastern boundary upwelling systems and increased
 184 stratification in the vicinity of major river mouths. On top of that, both parameters show
 185 a strong bathymetric dependence, as they are defined as vertical integrals.

186 These maps help to understand the horizontal distribution of the eddy dissipation timescale
 187 λ^{-1} (units in days) obtained from Equation 3 and shown in Figure 1c. Very short eddy
 188 timescales are found near the Gulf stream, the Kuroshio and the Agulhas regions as well
 189 as along the ACC. These geographical patterns were expected since they are also regions

190 of strong baroclinic currents. The same is also true along the north Atlantic subpolar gyre.
 191 As already pointed out in the horizontal stratification map, the short dissipation timescales
 192 found at high latitudes in the Arctic ocean and off Antarctica are doubtful. This result,
 193 although partly explained by the extremely weak vertical stratification in these regions,
 194 lacks of in-situ measurement and should be used with caution. Conversely, the dissipation
 195 timescale is large at low latitudes, in the equatorial regions and in the interior of subtropical
 196 gyres. Both the reduced horizontal shear and the high vertical stratification can explain the
 197 long eddy timescales found at those locations. To a lesser extent, a similar pattern is found
 198 in the north Pacific subpolar gyre.

199 This estimate can be compared to the work of Mak, Avdis, et al. (2022) who constrain the
 200 same eddy dissipation timescale using a kinematic inverse calculation inferred from an eddy
 201 permitting ocean circulation model. Similarly, short timescales are found near the western
 202 boundary currents and the ACC while subtropical gyre signatures are absent from their
 203 spatial distribution. Nevertheless, they find long dissipation timescales in eastern boundary
 204 regions, a feature less marked in our global estimation. In addition, within our eddy energy
 205 balance the eddy dissipation timescale is comparable with (although not equivalent to) the
 206 baroclinic growth rate. For instance, the eddy growth rate computed through a linear
 207 analysis by Tulloch et al. (2011) retrieves similar spatial patterns, even if the present work
 208 shows higher values at mid and low latitudes.

209 **3.3 Eddy Kinetic Energy Reconstruction**

210 From altimetry records, the surface eddy kinetic energy is computed and averaged between
 211 1995 and 2017. The resulting map is shown in Figure 2a. The western boundary currents,
 212 their extension, the ACC as well as the equatorial band show strong signatures with high
 213 levels of energy. The Indian Ocean also displays significant surface EKE while very weak
 214 levels are found at high latitudes, in the Arctic and next to the Antarctic, but also in the
 215 interior of subtropical gyres. The map is comparable to previous estimates of eddy kinetic
 216 energy also based on altimetry (Martinez-Moreno et al., 2020; Groeskamp et al., 2020).

217 Figure 2b shows the vertically-integrated EKE deduced from Equation 5. The use of the
 218 baroclinic surface mode vertical function clearly intensifies the eddy activity in the South-
 219 ern Ocean while weakening the energy patterns in the tropics and subtropics. The North
 220 Atlantic Current and the Labrador Sea also display deep vertical structures which in turn
 221 reinforce the integrated EKE near the Gulf Stream extension (see Figure S4 in the Support-
 222 ing Information). In addition, the bathymetry affects the final map and more particularly,
 223 almost no energy is found near the coasts nor in shallow waters.

224 Integrated over the whole domain, the total EKE reservoir accounts for 4.42 EJ (10^{18} J).
 225 For comparison with other studies based on high resolution models, von Storch et al. (2012)
 226 found 3.55 EJ while the work of Yu and Metzger (2019) estimated a smaller EKE reservoir
 227 of 1.76 EJ. These results therefore give credit to our method and the use of the surface mode
 228 vertical structure in the reconstruction of the geostrophic eddy field.

229 **3.4 Global Estimate of the Eddy Kinetic Energy Dissipation**

230 By combining the estimated eddy dissipation timescale and the vertical integral EKE, the
 231 dissipation rate of mesoscale kinetic energy is obtained and mapped in Figure 3. To some
 232 extent, the map retains the horizontal patterns of the integrated EKE (Figure 2b), although
 233 intensified. Indeed, boundary currents and the ACC are found to be highly dissipative
 234 regions of mesoscale eddies since they hold large levels of energy while also presenting
 235 short eddy dissipation timescales (Figure 1c). In the northern hemisphere, intense EKE
 236 dissipation is found in the Kuroshio as well as the Gulf Stream region and its extension. In
 237 the southern hemisphere, the Agulhas Current and its retroflexion, the Zapiola gyre and
 238 the ACC signatures are striking with an eddy dissipation rate often exceeding 25 mW/m^2 .

Table 1: Domain-integrated dissipation rate of the eddy kinetic energy over oceanic basins displayed in Figure 3. The longitude and latitude bounds for each box are also indicated as well as the associated ocean area. The ACC basin is defined following the mask created by Martinez-Moreno et al. (2020) but modified to include a part of the Agulhas retroflection between 52–100°E and southward to 42°S, while removing the boxes used for the southern boundary current. The surface average represents the ratio between the integrated dissipation rate and the basin area.

	Global	Gulf Stream	Kuroshio	Agulhas	Brazil-Malvinas	ACC
Longitude	-	73°-39°W	140°-175°E	14°-52°E	59.5°-32°W	-
Latitude	-	33°-44°N	30°-42°N	30°-44°S	34.5°-50.5°S	-
Surface area (10 ⁶ km ²)	344.3	3.5	4.1	4.7	4.1	66.6
% of total	(100 %)	(1.0 %)	(1.2 %)	(1.4 %)	(1.2 %)	(19.4 %)
Dissipation rate (TW)	0.66 ± 0.19	0.05 ± 0.01	0.03 ± 0.01	0.07 ± 0.02	0.03 ± 0.01	0.25 ± 0.04
% of total	(100 %)	(7.8 ± 2.7 %)	(4.5 ± 1.8 %)	(10.6 ± 3.9 %)	(5.0 ± 2.2 %)	(37.5 ± 12.8 %)
Surface average (mW/m ²)	1.93 ± 0.56	14.82 ± 2.85	7.26 ± 2.02	14.97 ± 3.42	8.06 ± 2.64	3.34 ± 0.60

239 The map also reveals both the East Australian Current and the West Australian Current
 240 as places of mesoscale EKE dissipation. The latter is the only ocean eastern boundary
 241 upwelling region present on this global map.

242 Intermediate levels of EKE dissipation are found in the equatorial and subtropical bands,
 243 mostly in the Pacific Ocean. Even if these regions are theoretically less prone to baroclinic
 244 instability (Tulloch et al., 2011), the amount of computed EKE and the simple balance of
 245 Equation 3 produce a relatively large eddy dissipation. This pattern is not often observed
 246 in previous studies (Sen et al., 2008; Xu et al., 2011) but reflects the large number of
 247 attendant eddies in these regions (Chelton et al., 2011). Finally, the dissipation rate shows
 248 strong variations zonally with very weak EKE removal in the Eastern part of ocean basins.
 249 In particular the North and South Pacific subtropical gyres have a pronounced signature
 250 with a minimum of EKE dissipation found in the vicinity of the Alaska, the California and
 251 the Humboldt Currents. Both the horizontal distribution of EKE and of the dissipation
 252 timescale explain these patterns.

253 Since most of the mesoscale dissipation occurs in strong and deep-reaching currents, domain-
 254 integrated EKE dissipation rates are computed over the most energetic ocean regions and
 255 summarized in Table 1. Covering only a small part of the global ocean area, the four main
 256 western boundary current systems are responsible here for more than 25% of the total EKE
 257 sinks. It is particularly true in the Agulhas and the Gulf Stream regions with an average
 258 dissipation rate of 15 mW/m², one order of magnitude larger than the global average.
 259 The southern hemisphere clearly dominates the EKE dissipation with numerous dissipation
 260 hotspots, notably in the ACC which cumulates more than a third of the global dissipation.

261 In total, we find a global EKE dissipation rate of 0.66 ± 0.19 TW. This figure represents a
 262 substantial fraction of the ~ 1 TW wind power input to the geostrophic field (Wunsch, 1998)
 263 and is close to the expected eddy potential to kinetic energy conversion rate (von Storch et
 264 al., 2012), confirming the key role of mesoscale eddies in the ocean energy cycle. Our results
 265 are also in the range of previous global estimations. Sen et al. (2008) computed an observed
 266 dissipation of geostrophic motion by bottom drag between 0.2 TW and 0.8 TW while Arbic
 267 et al. (2009) obtained a reduced range of 0.14-0.65 TW from different simulations. This
 268 finding suggests the bottom drag is a leading-order mechanism of mesoscale dissipation even
 269 if regional and cross-comparison studies are needed to better quantify the EKE dissipation
 270 processes.

271 4 Discussion

272 4.1 Validation of the Eddy Energy Balance

273 In section 2, a diagnostic eddy energy balance is presented where the energy sources by
 274 baroclinic instability are offset by a linear EKE dissipation. In this study, we use a coarse
 275 and global low-resolution model to verify this eddy energy balance. The simulation outputs
 276 tend to validate the framework but still indicate errors evaluated at 35%. These figures
 277 should be carefully interpreted since the model and the chosen parameterized energy budget
 278 necessarily present some biases. More precisely, the barotropic instability is neglected in
 279 Equation 1 although it could be a significant mechanism for the generation of mesoscale
 280 eddies (e.g. Gula et al., 2015; Maillard et al., 2022). However, at the global scale, model-
 281 based Lorenz energy cycle estimates suggest that baroclinic production by far exceeds its
 282 barotropic counterpart (von Storch et al., 2012). In addition, satellite observations have
 283 shown that eddies could efficiently propagate westward (Chelton et al., 2007, 2011; Zhai et
 284 al., 2010), indicating that advection may play a role in the EKE budget. Finally, recent
 285 studies indicate strong observed EKE variability (Ding et al., 2017; Martinez-Moreno et al.,
 286 2020) and possible long-term trends (Beech et al., 2022). Nonetheless, on the decadal time
 287 scale relatively small trends of EKE are found, supporting the hypothesis of a steady eddy
 288 kinetic energy reservoir. In order to account for all the aforementioned processes, eddy-rich
 289 and high-resolution models could be used to validate the eddy energy balance.

290 4.2 Sensitivity of the Eddy Dissipation to the Eddy Efficiency α

291 Another assumption in our method remains in the choice of the eddy efficiency α , and
 292 to our knowledge, there is no method to get an accurate estimation of this parameter
 293 in the global ocean. Bachman et al. (2017) use a suite of idealized channel simulations
 294 to compare several parameterizations of eddy transfer coefficients. They recommend the
 295 equilibrated long-term value of 0.2, even if the eddy efficiency takes different values during
 296 the eddy lifetime. Poulsen et al. (2019) diagnose the spatial structure of the eddy efficiency
 297 in the Southern Ocean with an eddy-resolving ocean circulation model. They recommend
 298 an average value as low as 0.043, consistent with the default value of 0.04 used in the
 299 GEOMETRIC parameterization (Mak et al., 2018; Mak, Marshall, et al., 2022). More
 300 recently, Wei et al. (2022) set the eddy efficiency to 0.07 in order to optimize their diagnostics
 301 of the eddy buoyancy fluxes in shelf and open ocean regions of eddy resolving simulations.

302 We also note that the eddy efficiency α in Equations 2 and 3 is different from the one
 303 introduced by Marshall et al. (2012) which use the total eddy energy instead of the EKE.
 304 However, the work of Bachman et al. (2017) suggests that switching the total to eddy kinetic
 305 energy in the scaling of κ_{gm} is physically consistent even if the coefficient should be increased
 306 by a given factor. Therefore, the above-mentioned values of the eddy efficiency should be
 307 increased when considering the EKE. Therefore we chose $\alpha = 0.1$ which is around twice the
 308 mean value diagnosed by Poulsen et al. (2019) in a realistic high-resolution model. Even
 309 if this value seems reasonable, we acknowledge the large uncertainties in our results due to
 310 the linear dependences of the EKE dissipation rate to α in the Equations 1 and 3. Indeed,
 311 taking extreme values of $\alpha = 0.04$ and $\alpha = 0.4$ would lead to a central estimate of 0.27 TW
 312 and 2.66 TW respectively, for the global EKE dissipation rate.

313 5 Conclusion

314 Dominating the ocean kinetic energy reservoir, mesoscale eddies are central to the Earth
 315 energy balance and transient climate response (Greatbatch et al., 2007; Chelton, 2013).
 316 Regarding the dissipation of this eddy kinetic energy (EKE), spatial distributions are still
 317 not well quantified in the global ocean. Indeed, direct and global measurements present

318 serious instrumental difficulties making the problem of estimating the global eddy dissipation
319 unsolved.

320 This present work proposes a global reconstruction of the EKE dissipation indirectly from
321 observations. A simplified model for the ocean mesoscale energetics is employed, where
322 baroclinic instability sources are perfectly balanced by sinks of EKE. In this model, the dis-
323 sipative mechanisms are interpreted by means of eddy dissipation timescales and are directly
324 related to the ocean stratification. The model and the energy balance were tested with an
325 oceanic global circulation simulation using a parameterized eddy energy prognostic equa-
326 tion. In the whole ocean domain, the dissipation of EKE tends to approach its production
327 by baroclinic instability, thereby confirming the adopted eddy energy balance. However, the
328 dissipation also dominates some part of the ocean where other processes impact the EKE
329 budget, illustrating the need for more realistic diagnostics of this eddy energy balance.

330 The framework is applied to available observations of temperature and salinity to compute
331 a global map of the eddy dissipation timescale. The shortest timescales (higher dissipation)
332 are found in the Southern Ocean and near strong western boundary currents coinciding with
333 the regions prone to high baroclinic instability and large eddy growth rates (Tulloch et al.,
334 2011). By projecting the eddy energy into depth using baroclinic surface modes (LaCasce
335 & Groeskamp, 2020), a three-dimensional EKE field is also computed where the mean EKE
336 reservoir is estimated to 4.42 EJ. Our work finally combines the two previous ingredients
337 and provides a new global map for the EKE dissipation rate. Integrated over the whole
338 ocean, the energy flux going out of the mesoscale reaches 0.66 ± 0.19 TW. Our study also
339 confirms that most of the energy dissipation takes place in the southern hemisphere and
340 more particularly in the Antarctic Circumpolar Current which accounts for 38% of the total
341 dissipation. In addition, the main western boundary currents are found to be dissipation
342 hotspots of EKE, accounting for more than 25% of the global dissipation.

343 Given the simplicity of the relation in Equation 3, the adopted framework allows an easy
344 computation of the global EKE dissipation rate from indirect observations. Indeed, the
345 method only requires a climatological mean field of density and surface geostrophic velocity
346 anomalies, both of these being widely available observational data. Our results show im-
347 portant spatial patterns which if combined with other independent estimates, can help to
348 understand the dissipation mechanisms. Since the dissipation of geostrophic kinetic energy
349 remains one of the largest uncertainties in the ocean energy budget (Wunsch, 2004), it is
350 thus crucial to quantify how and where the energy is removed from the EKE reservoir. Our
351 results contribute to this goal and provide a new spatial distribution of the EKE dissipation
352 rate in the world ocean.

353 Another important finding of this work is the estimation of the linear eddy dissipation
354 coefficient λ employed in several ocean models (Cessi, 2008; Marshall & Adcroft, 2010; Mak
355 et al., 2017, 2018). Recently, Mak, Marshall, et al. (2022) have demonstrated the sensitivity
356 of global ocean circulation models using energy constrained mesoscale eddy parameterization
357 to the eddy dissipation timescale λ^{-1} . In this study, we present the first estimate of the
358 eddy timescale from global observation-based datasets. The resulting map can thus be used
359 in eddy-parameterized ocean models to constrain the eddy energy dissipation and modulate
360 the ocean stratification.

361 **Open Research**

362 This study has been conducted using E.U. Copernicus Marine Service Information: <https://doi.org/10.48670/moi-00148> for the altimetry dataset. Both climatology of tempera-
363 ture (Locarnini et al., 2018) and salinity (Zweng et al., 2018) from the World Ocean At-
364 las 2018 were downloaded through the National Oceanic and Atmospheric Administration
365 website: <https://www.ncei.noaa.gov/archive/accession/NCEI-WOA18>, on 9 September
366

367 2022. Datas and Python scripts used to generate the results presented in this work are
 368 available on Zenodo : <https://sandbox.zenodo.org/record/1206326>.

369 **Acknowledgments**

370 This project has received support from the European Union’s Horizon 2020 research and
 371 innovation programme under Grant Agreement N° 101003536 (ESM2025 – Earth System
 372 Models for the Future). JM also acknowledges support from both the RGC Early Career
 373 Scheme 2630020 and the Center for Ocean Research in Hong Kong and Macau, a joint re-
 374 search center between the Qingdao National Laboratory for Marine Science and Technology
 375 and Hong Kong University of Science and Technology. The authors would like to thank
 376 Sjoerd Groeskamp for his review and useful comments, and Jean-Baptiste Sallée for the
 377 discussions about observational measurements that make improvements in this final version
 378 of the article.

379 **References**

- 380 Arbic, B. K., Shriver, J. F., Hogan, P. J., Hurlburt, H. E., McClean, J. L., Metzger, E. J.,
 381 ... Wallcraft, A. J. (2009, feb). Estimates of bottom flows and bottom boundary
 382 layer dissipation of the oceanic general circulation from global high-resolution models.
 383 *Journal of Geophysical Research*, *114*(C2). doi: 10.1029/2008jc005072
- 384 Bachman, S., Marshall, D., Maddison, J., & Mak, J. (2017). Evaluation of a scalar eddy
 385 transport coefficient based on geometric constraints. *Ocean Modelling*, *109*, 44–54.
 386 doi: 10.1016/j.ocemod.2016.12.004
- 387 Barkan, R., Winters, K. B., & Smith, S. G. L. (2015, jan). Energy cascades and loss of
 388 balance in a reentrant channel forced by wind stress and buoyancy fluxes. *Journal of*
 389 *Physical Oceanography*, *45*(1), 272–293. doi: 10.1175/JPO-D-14-0068.1
- 390 Beech, N., Rackow, T., Semmler, T., Danilov, S., Wang, Q., & Jung, T. (2022, sep). Long-
 391 term evolution of ocean eddy activity in a warming world. *Nature Climate Change*,
 392 *12*(10), 910–917. doi: 10.1038/s41558-022-01478-3
- 393 Braby, L., Backeberg, B. C., Anson, I., Roberts, M. J., Krug, M., & Reason, C. J. C.
 394 (2016, aug). Observed eddy dissipation in the Agulhas Current. *Geophysical Research*
 395 *Letters*, *43*(15), 8143–8150. doi: 10.1002/2016gl069480
- 396 Cessi, P. (2008, aug). An energy-constrained parameterization of eddy buoyancy flux.
 397 *Journal of Physical Oceanography*, *38*(8), 1807–1819. doi: 10.1175/2007JPO3812.1
- 398 Chelton, D. B. (2013, jul). Mesoscale eddy effects. *Nature Geoscience*, *6*(8), 594–595. doi:
 399 10.1038/ngeo1906
- 400 Chelton, D. B., Schlax, M. G., & Samelson, R. M. (2011, oct). Global observations of
 401 nonlinear mesoscale eddies. *Progress in Oceanography*, *91*(2), 167–216. doi: 10.1016/
 402 j.pocean.2011.01.002
- 403 Chelton, D. B., Schlax, M. G., Samelson, R. M., & de Szoeke, R. A. (2007, aug). Global
 404 observations of large oceanic eddies. *Geophysical Research Letters*, *34*(15). doi: 10
 405 .1029/2007gl030812
- 406 Cooley, S., Schoeman, D., Bopp, L., Boyd, P., Donner, S., Ghebrehiwet, D., ... Skern-
 407 Mauritzen, M. (2022). Oceans and coastal ecosystems and their services. in: Climat-
 408 exchange 2022: Impacts, adaptation and vulnerability. contribution of working group
 409 ii to the sixth assessment report of the intergovernmental panel on climate change. In
 410 H.-O. Pörtner et al. (Eds.), (p. 379–550). Cambridge University Press, Cambridge, UK
 411 and New York, NY, USA. Retrieved from [https://www.ipcc.ch/report/ar6/wg2/
 412 downloads/report](https://www.ipcc.ch/report/ar6/wg2/downloads/report)
- 413 Couldrey, M. P., Gregory, J. M., Dias, F. B., Dobrohotoff, P., Domingues, C. M., Garuba,
 414 O., ... Zanna, L. (2020, oct). What causes the spread of model projections of ocean
 415 dynamic sea-level change in response to greenhouse gas forcing? *Climate Dynamics*,
 416 *56*(1-2), 155–187. doi: 10.1007/s00382-020-05471-4

- 417 Ding, M., Lin, P., Liu, H., & Chai, F. (2017, dec). Increased eddy activity in the northeastern
 418 Pacific during 1993–2011. *Journal of Climate*, *31*(1), 387–399. doi: 10.1175/jcli-d-17-
 419 -0309.1
- 420 European Union-Copernicus Marine Service. (2021). *Global ocean gridded 1/4 sea surface*
 421 *heights and derived variables reprocessed (1993-ongoing)*. Mercator Ocean Interna-
 422 tional. doi: 10.48670/MOI-00148
- 423 Ferrari, R., & Wunsch, C. (2009, jan). Ocean circulation kinetic energy: Reservoirs, sources,
 424 and sinks. *Annual Review of Fluid Mechanics*, *41*(1), 253–282. doi: [http://dx.doi.org/
 425 10.1146/annurev.fluid.40.111406.102139](http://dx.doi.org/10.1146/annurev.fluid.40.111406.102139)
- 426 Firing, E., Filipe, Barna, A., & Abernathey, R. (2021). *Teos-10/gsw-python: v3.4.1*.
 427 Zenodo. Retrieved from <https://teos-10.github.io/GSW-Python/> doi: 10.5281/
 428 ZENODO.4631364
- 429 Fox-Kemper, B., Adcroft, A., Böning, C. W., Chassignet, E. P., Curchitser, E., Danabasoglu,
 430 G., ... Yeager, S. G. (2019, feb). Challenges and prospects in ocean circulation models.
 431 *Frontiers in Marine Science*, *6*. doi: 10.3389/fmars.2019.00065
- 432 Fox-Kemper, B., Hewitt, H., Xiao, C., Adalgeirsdóttir, G., Drijfhout, S., Edwards, T., ...
 433 Yu, Y. (2021). Ocean, cryosphere and sea level change. in climate change 2021:
 434 The physical science basis. contribution of working group i to the sixth assessment
 435 report of the intergovernmental panel on climate change. In M.-D. V. et al. (Eds.),
 436 (p. 1211–1362). Cambridge University Press, Cambridge, United Kingdom and New
 437 York, NY, USA. Retrieved from [https://www.ipcc.ch/report/ar6/wg1/chapter/
 438 chapter-9/](https://www.ipcc.ch/report/ar6/wg1/chapter/chapter-9/)
- 439 Friedlingstein, P., Jones, M. W., O'Sullivan, M., Andrew, R. M., Bakker, D. C. E., Hauck,
 440 J., ... Zeng, J. (2022, apr). Global carbon budget 2021. *Earth System Science Data*,
 441 *14*(4), 1917–2005. doi: 10.5194/essd-14-1917-2022
- 442 Garcia, H. E., Boyer, T. P., Baranova, O. K., Locarnini, R. A., Mishonov, A. V., Grodsky,
 443 A., ... Zweng, M. M. (2019). World Ocean Atlas 2018: Product documentation.
 444 NOAA National Centers for Environmental Information. Retrieved from [https://
 445 www.ncei.noaa.gov/archive/accession/NCEI-WO18](https://www.ncei.noaa.gov/archive/accession/NCEI-WO18)
- 446 Gent, P. R., & McWilliams, J. C. (1990, jan). Isopycnal mixing in ocean circula-
 447 tion models. *Journal of Physical Oceanography*, *20*(1), 150-155. doi: 10.1175/
 448 1520-0485(1990)020<0150:imiocm>2.0.co;2
- 449 Gent, P. R., Willebrand, J., McDougall, T. J., & McWilliams, J. C. (1995, apr). Parameter-
 450 izing eddy-induced tracer transports in ocean circulation models. *Journal of Physical*
 451 *Oceanography*, *25*(4), 463–474. doi: 10.1175/1520-0485(1995)025<0463:peitti>2.0.co;2
- 452 Greatbatch, R. J., Zhai, X., Eden, C., & Olbers, D. (2007, apr). The possible role in
 453 the ocean heat budget of eddy-induced mixing due to air-sea interaction. *Geophysical*
 454 *Research Letters*, *34*(7). doi: 10.1029/2007gl029533
- 455 Groeskamp, S., LaCasce, J. H., McDougall, T. J., & Rogé, M. (2020, sep). Full-depth global
 456 estimates of ocean mesoscale eddy mixing from observations and theory. *Geophysical*
 457 *Research Letters*, *47*(18). Retrieved from <https://doi.org/10.1029/2020GL089425>
 458 doi: 10.1029/2020gl089425
- 459 Gula, J., Molemaker, M. J., & McWilliams, J. C. (2015, mar). Gulf Stream dynamics along
 460 the southeastern U.S. seaboard. *Journal of Physical Oceanography*, *45*(3), 690–715.
 461 doi: 10.1175/jpo-d-14-0154.1
- 462 IOC, SCOR, & IAPSO. (2010). The international thermodynamic equation of seawater
 463 – 2010: Calculation and use of thermodynamic properties. In (p. 196). UNESCO
 464 (English).
- 465 Ji, J., Dong, C., Zhang, B., Liu, Y., Zou, B., King, G. P., ... Chen, D. (2018, nov).
 466 Oceanic eddy characteristics and generation mechanisms in the Kuroshio extension
 467 region. *Journal of Geophysical Research: Oceans*, *123*(11), 8548–8567. doi: 10.1029/
 468 2018jc014196
- 469 Klymak, J. M. (2018, oct). Nonpropagating form drag and turbulence due to stratified flow
 470 over large-scale abyssal hill topography. *Journal of Physical Oceanography*, *48*(10),
 471 2383–2395. doi: 10.1175/jpo-d-17-0225.1

- 472 Klymak, J. M., Balwada, D., Garabato, A. N., & Abernathey, R. (2021, may). Parameter-
 473 izing nonpropagating form drag over rough bathymetry. *Journal of Physical Oceanog-*
 474 *raphy*, *51*(5), 1489–1501. doi: 10.1175/jpo-d-20-0112.1
- 475 LaCasce, J. H., & Groeskamp, S. (2020, oct). Baroclinic modes over rough bathymetry and
 476 the surface deformation radius. *Journal of Physical Oceanography*, *50*(10), 2835–2847.
 477 doi: 10.1175/jpo-d-20-0055.1
- 478 Locarnini, R. A., Mishonov, A. V., Baranova, O. K., Boyer, T. P., Zweng, M. M., García,
 479 H. E., . . . Smolyar, I. (2018). World Ocean Atlas 2018, Volume 1: Temperature.
 480 *NOAA Atlas NESDIS*(81), 52.
- 481 Maillard, L., Boucharel, J., & Renault, L. (2022, aug). Direct and rectified effects of tropical
 482 instability waves on the eastern tropical Pacific mean state in a regional ocean model.
 483 *Journal of Physical Oceanography*, *52*(8), 1817–1834. doi: 10.1175/jpo-d-21-0300.1
- 484 Mak, J., Avdis, A., David, T., Lee, H. S., Na, Y., Wang, Y., & Yan, F. E. (2022). On
 485 constraining the mesoscale eddy energy dissipation time-scale. *Journal of Advances*
 486 *in Modeling Earth Systems*. doi: <https://doi.org/10.1029/2022MS003223>
- 487 Mak, J., Maddison, J. R., Marshall, D. P., & Munday, D. R. (2018, oct). Implementation of a
 488 geometrically informed and energetically constrained mesoscale eddy parameterization
 489 in an ocean circulation model. *Journal of Physical Oceanography*, *48*(10), 2363–2382.
 490 doi: 10.1175/jpo-d-18-0017.1
- 491 Mak, J., Marshall, D., Maddison, J., & Bachman, S. (2017, apr). Emergent eddy saturation
 492 from an energy constrained eddy parameterisation. *Ocean Modelling*, *112*, 125–138.
 493 doi: <http://dx.doi.org/10.1016/j.ocemod.2017.02.007>
- 494 Mak, J., Marshall, D. P., Madec, G., & Maddison, J. R. (2022, apr). Acute sensitivity
 495 of global ocean circulation and heat content to eddy energy dissipation timescale.
 496 *Geophysical Research Letters*, *49*(8). doi: 10.1029/2021GL097259
- 497 Marshall, D. P., & Adcroft, A. J. (2010, jan). Parameterization of ocean eddies: Potential
 498 vorticity mixing, energetics and Arnold’s first stability theorem. *Ocean Modelling*,
 499 *32*(3-4), 188–204. doi: 10.1016/j.ocemod.2010.02.001
- 500 Marshall, D. P., Ambaum, M. H. P., Maddison, J. R., Munday, D. R., & Novak, L. (2017,
 501 jan). Eddy saturation and frictional control of the Antarctic Circumpolar Current.
 502 *Geophysical Research Letters*, *44*(1), 286–292. doi: 10.1002/2016gl071702
- 503 Marshall, D. P., Maddison, J. R., & Berloff, P. S. (2012, apr). A framework for parameteriz-
 504 ing eddy potential vorticity fluxes. *Journal of Physical Oceanography*, *42*(4), 539–557.
 505 doi: 10.1175/jpo-d-11-048.1
- 506 Martinez-Moreno, J., Hogg, A., England, M., Constantinou, N. C., Kiss, A. E., & Morrison,
 507 A. (2020, oct). Global changes in oceanic mesoscale currents over the satellite altimetry
 508 record.
 509 doi: 10.21203/rs.3.rs-88932/v1
- 510 McWilliams, J. C. (2016, may). Submesoscale currents in the ocean. *Proceedings of the Royal*
 511 *Society A: Mathematical, Physical and Engineering Sciences*, *472*(2189), 20160117.
 512 doi: 10.1098/rspa.2016.0117
- 513 Melet, A., Hallberg, R., Adcroft, A., Nikurashin, M., & Legg, S. (2015, mar). Energy flux
 514 into internal lee waves: Sensitivity to future climate changes using linear theory and a
 515 climate model. *Journal of Climate*, *28*(6), 2365–2384. doi: 10.1175/jcli-d-14-00432.1
- 516 Molemaker, M. J., McWilliams, J. C., & Capet, X. (2010, jun). Balanced and unbalanced
 517 routes to dissipation in an equilibrated Eady flow. *Journal of Fluid Mechanics*, *654*,
 518 35–63. doi: 10.1017/S0022112009993272
- 519 Naveira Garabato, A. C., Polzin, K. L., King, B. A., Heywood, K. J., & Visbeck, M. (2004,
 520 jan). Widespread intense turbulent mixing in the southern ocean. *Science*, *303*(5655),
 521 210–213. doi: 10.1126/science.1090929
- 522 Nikurashin, M., & Ferrari, R. (2011, apr). Global energy conversion rate from geostrophic
 523 flows into internal lee waves in the deep ocean. *Geophysical Research Letters*, *38*(8).
 524 doi: 10.1029/2011GL046576
- 525 Polzin, K. L. (2010, apr). Mesoscale eddy–internal wave coupling. part II: Energetics
 526 and results from PolyMode. *Journal of Physical Oceanography*, *40*(4), 789–801. doi:

- 527 10.1175/2009jpo4039.1
- 528 Poulsen, M. B., Jochum, M., Maddison, J. R., Marshall, D. P., & Nuterman, R. (2019).
529 A geometric interpretation of southern ocean eddy form stress. *Journal of Physical*
530 *Oceanography*, *49*(10), 2553–2570. doi: 10.1175/JPO-D-18-0220.1
- 531 Rai, S., Hecht, M., Maltrud, M., & Aluie, H. (2021, jul). Scale of oceanic eddy killing
532 by wind from global satellite observations. *Science Advances*, *7*(28). doi: 10.1126/
533 sciadv.abf4920
- 534 Renault, L., Marchesiello, P., Masson, S., & McWilliams, J. C. (2019, mar). Remarkable
535 control of western boundary currents by *eddy killing*, a mechanical air-sea coupling
536 process. *Geophysical Research Letters*, *46*(5), 2743–2751. doi: 10.1029/2018gl081211
- 537 Robinson, A. R., & McWilliams, J. C. (1974, jul). The baroclinic instability of the
538 open ocean. *Journal of Physical Oceanography*, *4*(3), 281–294. doi: 10.1175/
539 1520-0485(1974)004(0281:TBIOTO)2.0.CO;2
- 540 Saenko, O. A., Yang, D., & Gregory, J. M. (2018, oct). Impact of mesoscale eddy transfer
541 on heat uptake in an eddy-parameterizing ocean model. *Journal of Climate*, *31*(20),
542 8589–8606. doi: 10.1175/jcli-d-18-0186.1
- 543 Saenko, O. A., Zhai, X., Merryfield, W. J., & Lee, W. G. (2012, apr). The combined effect of
544 tidally and eddy-driven diapycnal mixing on the large-scale ocean circulation. *Journal*
545 *of Physical Oceanography*, *42*(4), 526–538. doi: 10.1175/jpo-d-11-0122.1
- 546 Scott, R. B., Goff, J. A., Garabato, A. C. N., & Nurser, A. J. G. (2011, sep). Global rate and
547 spectral characteristics of internal gravity wave generation by geostrophic flow over
548 topography. *Journal of Geophysical Research*, *116*(C9). doi: 10.1029/2011jc007005
- 549 Sen, A., Scott, R. B., & Arbic, B. K. (2008, may). Global energy dissipation rate of
550 deep-ocean low-frequency flows by quadratic bottom boundary layer drag: Computa-
551 tions from current-meter data. *Geophysical Research Letters*, *35*(9). doi: 10.1029/
552 2008GL033407
- 553 Sun, M., Tian, F., Liu, Y., & Chen, G. (2017, feb). An improved automatic algorithm for
554 global eddy tracking using satellite altimeter data. *Remote Sensing*, *9*(3), 206. doi:
555 10.3390/rs9030206
- 556 Tulloch, R., Marshall, J., Hill, C., & Smith, K. S. (2011, jun). Scales, growth rates, and
557 spectral fluxes of baroclinic instability in the ocean. *Journal of Physical Oceanography*,
558 *41*(6), 1057–1076. doi: 10.1175/2011jpo4404.1
- 559 von Schuckmann, K., Cheng, L., Palmer, M. D., Hansen, J., Tassone, C., Aich, V., ...
560 Wijffels, S. E. (2020, sep). Heat stored in the earth system: where does the energy
561 go? *Earth System Science Data*, *12*(3), 2013–2041. doi: 10.5194/essd-12-2013-2020
- 562 von Storch, J.-S., Eden, C., Fast, I., Haak, H., Hernández-Deckers, D., Maier-Reimer, E.,
563 ... Stammer, D. (2012, dec). An estimate of the Lorenz energy cycle for the world
564 ocean based on the STORM/NCEP simulation. *Journal of Physical Oceanography*,
565 *42*(12), 2185–2205. doi: <https://doi.org/10.1175/JPO-D-12-079.1>
- 566 Wei, H., Wang, Y., Stewart, A. L., & Mak, J. (2022, dec). Scalings for eddy buoyancy fluxes
567 across prograde shelf/slope fronts. *Journal of Advances in Modeling Earth Systems*,
568 *14*(12). doi: 10.1029/2022ms003229
- 569 Wunsch, C. (1998, nov). The work done by the wind on the oceanic general circulation.
570 *Journal of Physical Oceanography*, *28*(11), 2332–2340. doi: 10.1175/1520-0485(1998)
571 028(2332:twdbtw)2.0.co;2
- 572 Wunsch, C. (2004, jan). Vertical mixing, energy, and the general circulation of the oceans.
573 *Annual Review of Fluid Mechanics*, *36*(1), 281–314. doi: 10.1146/annurev.fluid.36
574 .050802.122121
- 575 Xu, C., Shang, X.-D., & Huang, R. X. (2011, feb). Estimate of eddy energy genera-
576 tion/dissipation rate in the world ocean from altimetry data. *Ocean Dynamics*, *61*(4),
577 525–541. doi: 10.1007/s10236-011-0377-8
- 578 Yang, Q., Nikurashin, M., Sasaki, H., Sun, H., & Tian, J. (2019, jan). Dissipation of
579 mesoscale eddies and its contribution to mixing in the northern South China Sea.
580 *Scientific Reports*, *9*(1). doi: 10.1038/s41598-018-36610-x

- 581 Yu, Z., & Metzger, E. J. (2019, jul). The impact of ocean surface currents on global eddy
582 kinetic energy via the wind stress formulation. *Ocean Modelling*, *139*, 101399. doi:
583 10.1016/j.ocemod.2019.05.003
- 584 Zanna, L., Khatiwala, S., Gregory, J. M., Ison, J., & Heimbach, P. (2019, jan). Global recon-
585 struction of historical ocean heat storage and transport. *Proceedings of the National*
586 *Academy of Sciences*, *116*(4), 1126–1131. doi: 10.1073/pnas.1808838115
- 587 Zhai, X., Johnson, H. L., & Marshall, D. P. (2010, aug). Significant sink of ocean-eddy
588 energy near western boundaries. *Nature Geoscience*, *3*(9), 608–612. doi: [https://](https://doi.org/10.1038/ngeo943)
589 doi.org/10.1038/ngeo943
- 590 Zweng, M. M., Reagan, J. R., Seidov, D., Boyer, T. P., Locarnini, R. A., García, H. E.,
591 ... Smolyar, I. (2018). World Ocean Atlas 2018, Volume 2: Salinity. *NOAA Atlas*
592 *NESDIS*(82), 50.

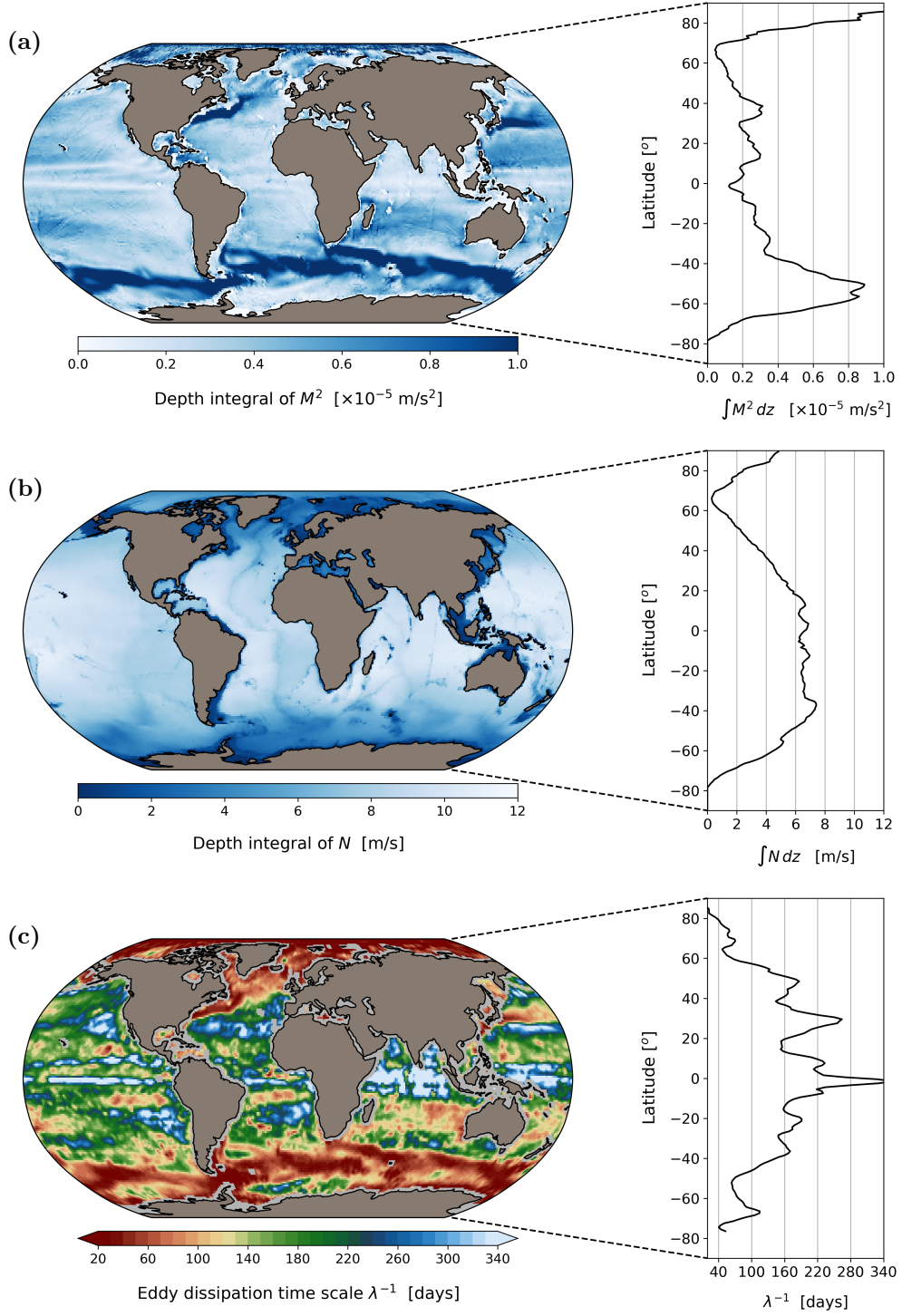


Figure 1: Depth integrals of (a) the horizontal buoyancy stratification M^2 (m/s^2) and (b) the Brunt-Väisälä frequency N (m/s) from the WOA18 climatology (Garcia et al., 2019). Equation 3 is used to compute (c) the global map of the eddy dissipation timescale λ^{-1} involving the ratio M^2/N while zonal averages are plotted on the right. In (a, b), the colormap is chosen so that dark blue leads to an increase of the eddy dissipation coefficient λ and conversely for light blue. In (c), we use a two-dimensional shapiro filter to reduce spatial noise.

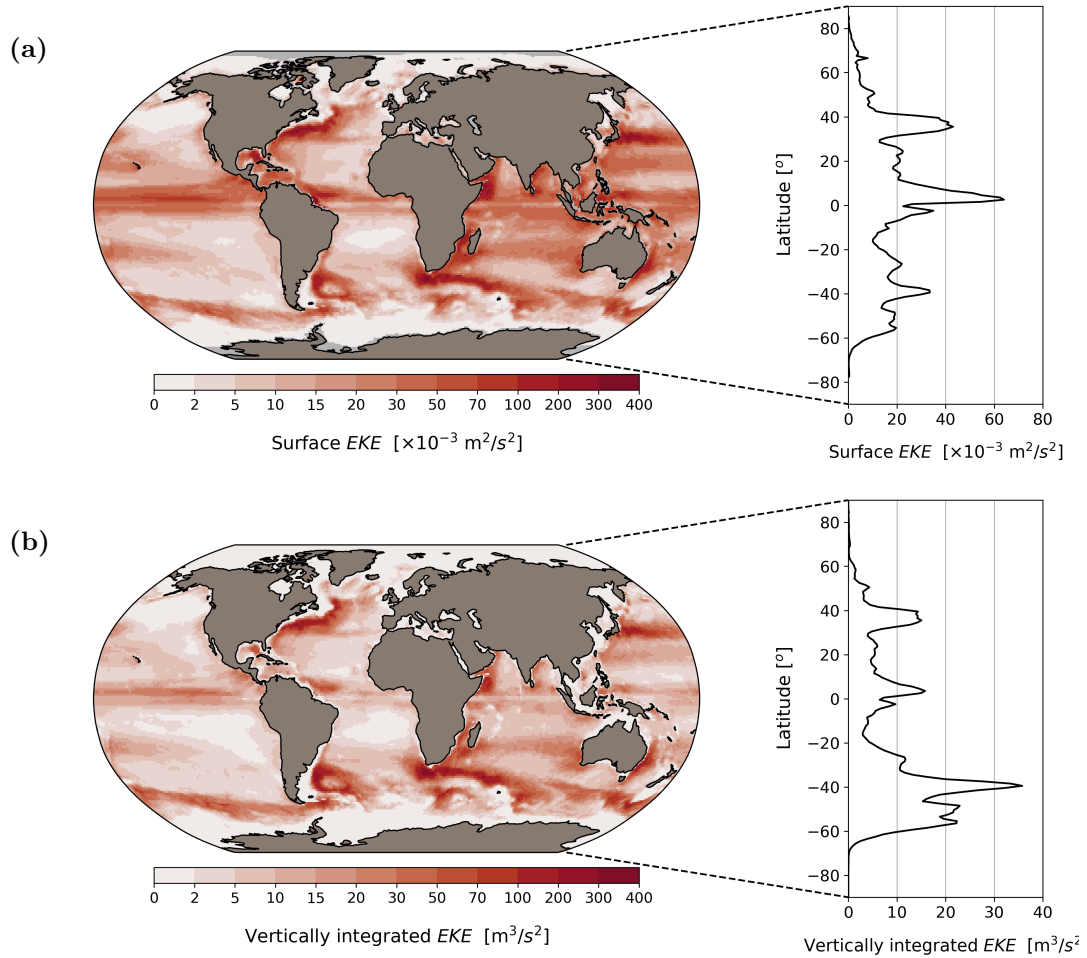


Figure 2: (a) Surface eddy kinetic energy (EKE) in m^2/s^2 deduced from the gridded altimetry (European Union-Copernicus Marine Service, 2021) and averaged over the period 1995–2017. (b) Vertically integrated EKE in m^3/s^2 deduced from the vertical structure function $\phi(z)$ in Equation 5. Both colorbars are chosen to illustrate the impact of $\phi(z)$ when computing the depth integral of EKE.

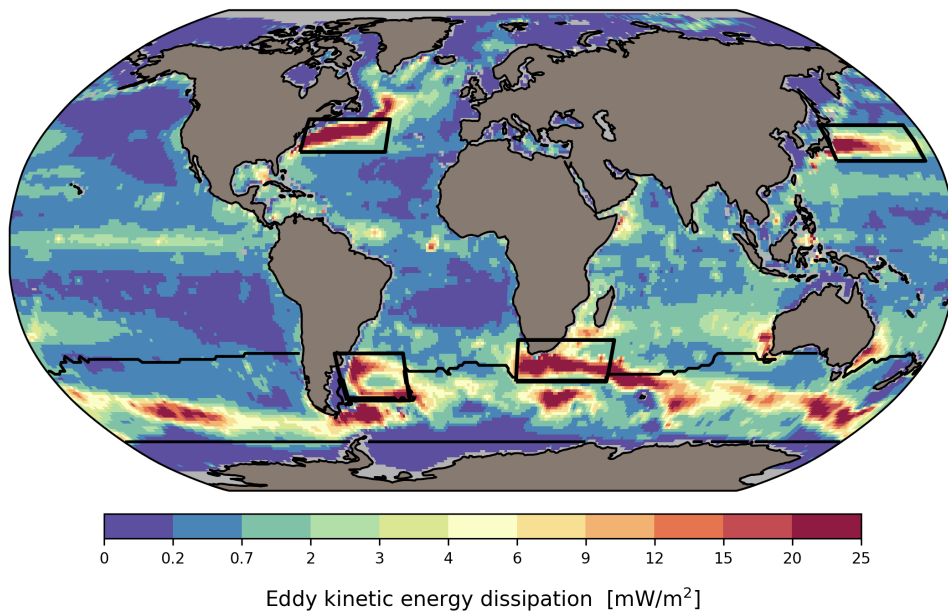


Figure 3: Vertically-integrated eddy dissipation rate in mW/m^2 estimated from the WOA18 climatology (Garcia et al., 2019) and the gridded altimetry (European Union-Copernicus Marine Service, 2021) over the period 1995–2017, with the use of the diagnostic relation in Equation 3. A reference density $\rho_0 = 1026 \text{ kg/m}^3$ is used and the black boxes refer to the ocean basins defined in Table 1.